

# 1 The germline mutational process in rhesus macaque 2 and its implications for phylogenetic dating

3  
4 Lucie A. Bergeron <sup>1\*</sup>, Søren Besenbacher <sup>2</sup>, Jaco Bakker <sup>3</sup>, Jiao Zheng <sup>4,5</sup>, Panyi Li <sup>4</sup>, George  
5 Pacheco <sup>6</sup>, Mikkel-Holger S. Sinding <sup>7,8</sup>, Maria Kamilari <sup>1</sup>, M. Thomas P. Gilbert <sup>6,9</sup>, Mikkel H.  
6 Schierup <sup>10</sup> and Guojie Zhang <sup>1,4,11,12\*</sup>

7  
8 <sup>1</sup> Section for Ecology and Evolution, Department of Biology, University of Copenhagen,  
9 Copenhagen, Denmark

10 <sup>2</sup> Department of Molecular Medicine, Aarhus University, Aarhus, Denmark

11 <sup>3</sup> Animal Science Department, Biomedical Primate Research Centre, Rijswijk, Netherlands

12 <sup>4</sup> BGI-Shenzhen, Shenzhen 518083, Guangdong, China

13 <sup>5</sup> BGI Education Center, University of Chinese Academy of Sciences, Shenzhen 518083,  
14 Guangdong, China

15 <sup>6</sup> Section for Evolutionary Genomics, The GLOBE Institute, University of Copenhagen,  
16 Copenhagen, Denmark

17 <sup>7</sup> Trinity College Dublin, Dublin, Ireland

18 <sup>8</sup> Greenland Institute of Natural Resources, Nuuk, Greenland

19 <sup>9</sup> Department of Natural History, NTNU University Museum, Norwegian University of Science  
20 and Technology (NTNU), NO-7491 Trondheim, Norway

21 <sup>10</sup> Bioinformatics Research Centre, Aarhus University, Aarhus, Denmark

22 <sup>11</sup> State Key Laboratory of Genetic Resources and Evolution, Kunming Institute of Zoology,  
23 Chinese Academy of Sciences, Kunming 650223, China

24 <sup>12</sup> Center for Excellence in Animal Evolution and Genetics, Chinese Academy of Sciences,  
25 Kunming 650223, China

26  
27 <sup>\*</sup> Corresponding author

28 E-mail: guojie.zhang@bio.ku.dk or lucie.a.bergeron@gmail.com

31 **Abstract**

32

33 Understanding the rate and pattern of germline mutations is of fundamental importance for  
34 understanding evolutionary processes. Here we analyzed 19 parent-offspring trios of rhesus  
35 macaques (*Macaca mulatta*) at high sequencing coverage of ca. 76X per individual, and  
36 estimated an average rate of  $0.77 \times 10^{-8}$  *de novo* mutations per site per generation (95 %  
37 CI:  $0.69 \times 10^{-8}$  -  $0.85 \times 10^{-8}$ ). By phasing 50 % of the mutations to parental origins, we found  
38 that the mutation rate is positively correlated with the paternal age. The paternal lineage  
39 contributed an average of 81 % of the *de novo* mutations, with a trend of an increasing male  
40 contribution for older fathers. About 3.5 % of *de novo* mutations were shared between siblings,  
41 with no parental bias, suggesting that they arose from early development (postzygotic) stages.  
42 Finally, the divergence times between closely related primates calculated based on the yearly  
43 mutation rate of rhesus macaque generally reconcile with divergence estimated with molecular  
44 clock methods, except for the Cercopithecidae/Hominoidea molecular divergence dated at 52  
45 Mya using our new estimate of the yearly mutation rate.

46

47 **Introduction**

48

49 Germline mutations are the source of heritable disease and evolutionary adaptation. Thus, having  
50 precise estimates of germline mutation rates is of fundamental importance for many fields in  
51 biology, including searching for *de novo* disease mutations (Acuna-Hidalgo et al. 2016; Oliveira  
52 et al. 2018), inferring demographic events (Lapierre et al. 2017; Zeng et al. 2018), and accurate  
53 dating of species divergence times (Teeling et al. 2005; Ho and Larson 2006; Pulquério and  
54 Nichols 2007). Over the past ten years, new sequencing techniques have allowed deep  
55 sequencing of individuals from the same pedigree, enabling direct estimation of the *de novo*  
56 mutation rate for each generation, and precise estimation of the individual parental contributions  
57 to germline mutations across the whole genome. Most such studies have been conducted on  
58 humans, using large pedigrees with up to 3000 trios (Jónsson et al. 2017; Halldorsson et al.  
59 2019), leading to a consensus estimate of  $\sim 1.25 \times 10^{-8}$  *de novo* mutation per site per generation,

60 with an average parental age of ~ 29 years, leading to a yearly rate of  $0.43 \times 10^{-9}$  *de novo*  
61 mutation per site per year and most variation between trios explained by the age of the parents  
62 (Awadalla et al. 2010; Roach et al. 2010; Kong et al. 2012; Neale et al. 2012; Wang and Zhu  
63 2014; Besenbacher et al. 2015; Rahbari et al. 2016; Jónsson et al. 2017; Maretty et al. 2017).  
64 The observed increases in the mutation rate with paternal age in humans and other primates  
65 (Venn et al. 2014; Jónsson et al. 2017; Thomas et al. 2018) has generally been attributed to  
66 errors during replication (Li et al. 1996; Crow 2000). In mammalian spermatogenesis, primordial  
67 germ cells go through meiotic divisions, to produce stem cells by the time of puberty. After this  
68 time, stem cell divisions occur continuously throughout the male lifetime. Thus, human  
69 spermatogonial stem cells have undergone 100 to 150 mitoses in a 20 years old male, and ~ 610  
70 mitoses in a 40 years old male (Acuna-Hidalgo et al. 2016), leading to an additional 1.51 *de novo*  
71 mutations per year increase in the father's age (Jónsson et al. 2017). Female age also seems to  
72 affect the mutation rate in humans, with 0.37 mutations added per year (Jónsson et al. 2017).  
73 This maternal effect cannot be attributed to replication errors, as different from spermatogenesis,  
74 female oocytogenesis occurs during embryogenesis process and is already finished before birth  
75 (Byskov 1986). Moreover, there seems to be a bias towards males in contribution to *de novo*  
76 mutations, as the paternal to maternal contribution is 4:1 in human and chimpanzee (Venn et al.  
77 2014; Jónsson et al. 2017). One recent study proposed that damage-induced mutations might be a  
78 potential explanation for the observation of both the maternal age effect and the male-bias also  
79 present in parents reproducing right after puberty when replication mutations should not have  
80 accumulated yet in the male germline (Gao et al. 2019). Parent-offspring analyses can also be  
81 used to distinguish mutations that are caused by gametogenesis from mutations that emerge in  
82 postzygotic stages (Acuna-Hidalgo et al. 2015; Scally 2016). While germline mutations in  
83 humans are relatively well studied, it remains unknown how much variability exists among  
84 primates on the contribution of replication errors to *de novo* mutations, the parental effects, and  
85 the developmental stages at which these mutations are established (postzygotic or  
86 gametogenesis).

87 Up until now, the germline mutation rate has only been estimated using pedigrees in few non-  
88 human primate species, including chimpanzee (*Pan troglodytes*) (Venn et al. 2014; Tatsumoto et  
89 al. 2017; Besenbacher et al. 2019), gorilla (*Gorilla gorilla*) (Besenbacher et al. 2019), orangutan

90 (*Pongo abelii*) (Bessenbacher et al. 2019), African green monkey (*Chlorocebus sabaeus*) (Pfeifer  
91 2017), owl monkey (*Aotus nancymaae*) (Thomas et al. 2018) and recently rhesus macaque  
92 (*Macaca mulatta*) (Wang et al. 2020). The mutation rate of baboon (*Papio anubis*) (Wu et al.  
93 2019) and grey mouse lemur (*Microcebus murinus*) (Campbell et al. 2019) have also been  
94 estimated in preprinted studies. To precisely call *de novo* mutations in the offspring, collecting  
95 and comparing the genomic information of the pedigrees is a first essential step for detecting  
96 mutations only present in offspring but not in either parent. Next, the *de novo* mutations need to  
97 be separated from sequencing errors or somatic mutations, which cause false-positive calls.  
98 Because mutations are rare events, detecting *de novo* mutations that occur within a single  
99 generation requires high sequencing coverage in order to cover a majority of genomic regions  
100 and identify the false-positives. Furthermore, the algorithms used to estimate the mutation rate  
101 should take false-negative calls into account. However, a considerable range of sequencing depth  
102 (ranging from 18X (Pfeifer 2017) to 120X (Tatsumoto et al. 2017)) has been applied in many  
103 studies for estimation of mutation rate. Different filtering methods have been introduced to  
104 reduce false-positives and false-negatives but the lack of standardized methodology makes it  
105 difficult to assess whether differences in mutation rate estimates are caused by technical or  
106 biological variability. In addition, most studies on non-human primates used small pedigrees  
107 with less than ten trios, which made it difficult to detect any statistically significant patterns over  
108 *de novo* mutation spectra.

109 Studying non-human primates could help us understanding whether the mutation rate is affected  
110 by life-history traits such as mating strategies or the age of reproduction. The variation in  
111 mutation rate among primates will also be useful for re-calibrating the speciation times across  
112 lineages. The sister group of Hominoidea is Cercopithecidae, including the important biomedical  
113 model species, rhesus macaque (*Macaca mulatta*), which share 93 % of its genome with humans  
114 (Gibbs et al. 2007). This species has a generation time estimate of ~ 11 years (Xue et al. 2016),  
115 and their sexual maturity is much earlier than in humans with females reaching maturity around  
116 three years old, while males mature around the age of 4 years (Rawlins and Kessler 1986). While  
117 female macaques generally start reproducing right after maturation, males rarely reproduce in the  
118 wild until they reach their adult body size, at approximately eight years old (Bercovitch et al.  
119 2003). They are also a promiscuous species, and do not form pair bonds, but reproduce with

120 multiple individuals. These life-history traits, along with their status as the closest related  
121 outgroup species of the hominoid group, make the rhesus macaque an interesting species for  
122 investigating the differences and common features in mutation rate processes across primates.  
123 In this study, we, produced high depth sequencing data for 33 rhesus macaque individuals (76X  
124 per individual) representing 19 trios. This particular dataset consists of a large number of trios,  
125 each with high coverage sequencing, and allowed us to test different filter criteria and choose the  
126 most appropriate ones to estimate the species mutation rate with high confidence. With a large  
127 number of *de novo* mutations phased to their parents of origins, we can statistically assess the  
128 parental contribution and the effect of the parental age. We characterize the type of mutations  
129 and their location on the genome to detect clusters and shared mutations between siblings.  
130 Finally, we use our new estimate to infer the effective population size and date their divergence  
131 time from closely related primate species.

132

## 133 **Results**

134

### 135 **Estimation of mutation rate for 19 trios of rhesus macaques**

136 To produce an accurate estimate for the germline mutation rate of rhesus macaques, we  
137 generated high coverage (76 X per individual after mapping, min 64 X, max 86 X) genome  
138 sequencing data for 19 trios of two unrelated families (Fig 1). The first family consisted of two  
139 reproductive males and four reproductive females, and the second family had one reproductive  
140 male and seven reproductive females. In the first family, the pedigree extended over a third  
141 generation in two cases. The promiscuous mating system of rhesus macaques allowed us to  
142 follow the mutation rates in various ages of reproduction, and compare numerous full siblings  
143 and half-siblings.

144 We developed a pipeline for single nucleotide polymorphisms (SNP) calling with multiple  
145 quality control steps involving the filtering of reads and sites (see Methods). For each trio, we  
146 considered candidate sites as *de novo* mutations when i) both parents were homozygotes for the  
147 reference allele, while the offspring was heterozygous with 30 % to 70 % of its reads supporting  
148 the alternative allele, and ii) the three individuals passed the depth and genotype quality filters (see

149 Methods). These filters were calibrated to ensure a low rate of false-positives among the  
150 candidate *de novo* mutations.

151 We obtained an unfiltered set of 12,785,386 average candidate autosomal SNPs per trio (se =  
152 26,196), of which a total of 177,227 were potential Mendelian violations (average of 9,328 per  
153 trio; se= 106). Of these, 744 SNPs passed the filters as *de novo* mutations, ranging from 25 to 59  
154 for each trio and an average of 39 *de novo* mutations per trio (se = 2) (see S1 Table). We  
155 manually curated all mutations using IGV on bam files and found that 663 mutations  
156 convincingly displayed as true positives. This leaves a maximum of 10.89 % (81 sites) that could  
157 be false-positives due to the absence of the variant in the offspring or presence of the variant in  
158 the parents (see S1 Fig and the 81 curated mutations in supplementary). Most of those sites were  
159 in dinucleotide repeat regions or short tandem repeats (56 sites), while others were in non-  
160 repetitive regions of the genome (25 sites). The manual curation may have missed the  
161 realignment executed during variant calling. Thus, in the absence of objective filters, we decided  
162 to keep these regions in the estimate of mutation rate but corrected the number of mutations for  
163 each trio with a false-positive rate (see equation 1 in Methods section).

164 To confirm the authenticity of the *de novo* mutations, we performed PCR experiments for all  
165 candidate *de novo* mutations from one trio before manual correction. We designed primers to a  
166 set of 39 *de novo* candidates among which 3 *de novo* mutations assigned as spurious from the  
167 manual inspection. Of these, 24 sites were successfully amplified and sequenced for all three  
168 individuals i.e mother, father, and offspring, including 1 of the spurious sites. Among those  
169 sequenced sites, 23 were correct, only one was wrong (S2 Fig). This invalidated candidate was  
170 the spurious candidate removed by manual curation, therefore supporting our manual curation  
171 method. The PCR validation results suggested a lower false-positive rate of 4.2 % before manual  
172 curation. As the PCR validation was done only on 24 candidates we decided to keep a strict  
173 false-positive rate of 10.89 % found by manual curation.

174 We then estimated the mutation rate, per site per generation, as the number of mutations  
175 observed, and corrected for false-positive calls, divided by the number of callable sites. The  
176 number of callable sites for each trio ranged from 2,334,764,487 to 2,359,040,186, covering on  
177 average 88 % of the autosomal sites of the rhesus macaque genome. A site was defined as

178 callable when both parents were homozygotes for the reference allele, and all individuals passed  
179 the depth and genotype quality filters at that site. As callability is determined using the base-pair  
180 resolution vcf file, containing every single site of the genome, all filters used during calling were  
181 taken into account during the estimation of callability, except for the site filters and the allelic  
182 balance filter. We then corrected for false-negative rates, calculated as the number of “good”  
183 sites that could be filtered away by both the site filters and allelic balance filters - estimated at  
184 4.02 % (see equation 1 in Methods section). Another method to estimate the false-negative rate  
185 is to simulate mutations on the bam files and evaluate the detection rate after passing through all  
186 filters. On 552 randomly simulated mutations among the 19 offsprings, 545 were detected as *de*  
187 *novo* mutations, resulting in a false-negative rate of 1.27 %. The 7 remaining mutations were  
188 filtered away by the allelic balance filter only, which can be explained by the reads filtering in  
189 the variant calling step. This result might be underestimated due to the methodological limitation  
190 of simulating *de novo* mutations, yet, it ensures that a false-negative rate of 4.02 % is not out of  
191 range. Thus, the final estimated average mutation rate of the rhesus macaques was  $0.77 \times 10^{-8}$  *de*  
192 *novo* mutations per site per generation (95 % CI  $0.69 \times 10^{-8}$  -  $0.85 \times 10^{-8}$ ). We removed the 81  
193 sites that, based on manual curation, could represent false-positive calls from the following  
194 analyses (see the 663 *de novo* mutations in S2 Table).

195

## 196 Parental contribution and age impact to the *de novo* mutation rate

197 We observed a positive correlation between the paternal age and the mutation rate in the  
198 offspring (adjusted  $R^2 = 0.23$ ;  $P = 0.021$ ; regression:  $\mu = 1.022 \times 10^{-9} + 5.393 \times 10^{-10} \times$   
199  $age_{paternal}$ ;  $P = 0.021$ ; Fig 2A). We also detected a slight positive correlation with the maternal  
200 age, though not significant (adjusted  $R^2 = 0.09$ ;  $P = 0.111$ ; regression:  $\mu = 6.200 \times 10^{-9} + 1.818 \times$   
201  $10^{-10} \times age_{maternal}$ ;  $P = 0.111$ ; Fig 2B). A multiple regression of the mutation rate on paternal and  
202 maternal age resulted in this formula:  $\mu_{Rhesus} = 1.355 \times 10^{-9} + 7.936 \times 10^{-11} \times age_{maternal} + 4.588 \times$   
203  $10^{-10} \times age_{paternal}$  ( $P = 0.06$ ), where  $\mu_{Rhesus}$  is the mutation rate for the species.  
204 We were able to phase 337 mutations to their parent of origin, which accounted for more than  
205 half of the total number of *de novo* mutations (663). There is a significant male bias in the

206 contribution of *de novo* mutations, with an average of 80.6 % paternal *de novo* mutations (95 %  
207 CI 76.6 % - 84.6 %;  $T = 22.62$ ,  $DF = 36$ ,  $P < 2.2 \times 10^{-16}$ ; Fig 2C). Moreover, with more than half  
208 of the *de novo* mutations phased to their parent of origin, we were able to disentangle the effect  
209 of the age of each parent on mutation rate independently (Fig 2D). By assuming that the ratio of  
210 mutations phased to a particular parent was the same in the phased mutations than in the  
211 unphased ones, we could predict the total number of mutations given by each parent. For  
212 instance, if an offspring had 40 *de novo* mutations and only half were phased, with 80 % given  
213 from its father, we would apply this ratio to the total number of mutations in this offspring,  
214 ending up with 32 *de novo* mutations from its father and eight from its mother. This analysis  
215 suggested a stronger male age effect to the number of mutations (adjusted  $R^2 = 0.41$ ,  $P = 0.002$ ),  
216 and a similar, non significant maternal age effect (adjusted  $R^2 = -0.01$ ,  $P = 0.38$ ). The two  
217 regression lines meet around the age of sexual maturity (3 years for females and 4 years for  
218 males), which is consistent with a similar accumulation of *de novo* mutations during the  
219 developmental process from birth to sexual maturity in both sexes, but the variances on the  
220 regression line slopes are large (see Fig 2C and S3 Fig for the same analysis with a Poisson  
221 regression). Using these two linear regressions, we can predict the number of *de novo* mutations  
222 in the offspring based on the age of each parent at the time of reproduction:  $nb\ of\ mutations\ Rhesus$   
223  $= 4.6497 + 0.3042 \times age_{maternal} + 4.8399 + 1.8364 \times age_{paternal}$ , where  $nb\ of\ mutations\ Rhesus$  is the  
224 number of *de novo* mutations for the given trio. The expected mutation rates calculated using the  
225 two different regression models show similar correlations with the observed mutation rate ( $R^2 =$   
226 0.54,  $P = 0.016$  for the first regression and  $R^2 = 0.54$ ,  $P = 0.016$  for the upscaled one, see S4 Fig).  
227 However, on the first regression on the mutation rate, the maternal age effect may be confounded  
228 by the paternal age, as maternal and paternal age are correlated in our dataset, yet, non-  
229 significantly ( $R^2 = 0.38$ ,  $P = 0.106$ , see S5 Fig). The upscaled regression unravels the effect of  
230 the parental age independently from each other. This regression can also be used to infer the  
231 contribution of each parent at different reproductive age. For instance, if both parents reproduce  
232 at 5 years old, based on the upscaled regression, the father is estimated to give  $\sim 14$  *de novo*  
233 mutations (95 % CI:6 - 22) and the mother  $\sim 6$  *de novo* mutations (95 % CI:3 - 10),  
234 corresponding to a contribution ratio from father to mother of 2.3:1 at 5 years old. If they  
235 reproduce at 15 years old, this ratio would be 3.6:1 with males giving  $\sim 32$  *de novo* mutations

236 (95 % CI: 29 – 36) and females ~ 9 *de novo* mutations (95 % CI: 4 – 14). It seems that the male  
237 bias increases with the parental age, yet, our model was based on too few data points in early  
238 male reproductive ages to reach a firm conclusion. For the two extended trios for which a second  
239 generation is available, we looked at the proportion of *de novo* mutations in the first offspring  
240 that were passed on to the third generation - the third generation inherited a heterozygote  
241 genotype with the alternative allele being the *de novo* mutation. In one case, 66 % of the *de novo*  
242 mutations in the female (Heineken) were passed to her daughter (Hoegaarde), while in another  
243 case, 40 % of the *de novo* mutations in the female (Amber) were passed to her son (Magenta).  
244 These deviations from the expected 50 % inheritance rate are not statistically significant  
245 (Binomial test;  $P_{\text{Hoegaarde}} = 0.14$  and  $P_{\text{Magenta}} = 0.27$ ).

246

#### 247 **Characterizations of *de novo* mutations**

248 We characterized the type of *de novo* mutations and found that transition from a strong base to  
249 weak base ( $G > A$  and  $C > T$ ) were most common (332/663), with 43 % of those mutations  
250 located in CpG sites (Fig 3A). In total, 23.2 % (154/663) of the *de novo* mutations were located in  
251 CpG sites. This is slightly higher than what has been found in humans, for which 19 % of the *de*  
252 *novo* mutations are in CpG sites (Besenbacher et al. 2015), but not significantly (human:  $\chi^2 =$   
253 2.774,  $df = 1$ ,  $P = 0.096$ ). Moreover, 32.1 % (144/448) of the transition mutations ( $A > G$  and  $C$   
254  $> T$ ) were in CpG sites, higher than what has been found in chimpanzee, with 24 % of the  
255 transition *de novo* mutations in CpG sites (Venn et al. 2014). The transition to transversion ratio  
256 (ti/tv) was 2.08, which is similar to the ratio observed in other species (human: ti/tv ~ 2.16 (Yuen  
257 et al. 2016); human ti/tv ~ 2.2 (Wang and Zhu 2014); chimpanzee: ti/tv ~ 1.98 (Tatsumoto et al.  
258 2017). The 663 *de novo* mutations showed some clustering in the genome (Fig 3B and S6 Fig).  
259 Across all trios, we observed 11 clusters, defined as windows of 20,000 bp where more than one  
260 mutation occurred in any individual, involving 23 mutations. Four clusters were made of  
261 mutations from a single individual, accounting for eight mutations (Fig 3B). Overall, 3.47 % of  
262 the *de novo* mutations were located in clusters, and 1.21 % were mutations within the same  
263 individual located in a cluster, which is significantly lower than the 3.1 % reported in humans  
264 (Besenbacher et al. 2016) ( $\chi^2 = 7.35$ ,  $DF = 1$ ,  $P = 0.007$ ; S7 Fig, S3 Table). We observed 23

265 mutations occurring recurrently in more than one related individual (Table 1), which accounted  
266 for 3.5 % of the total number of *de novo* mutations (23/663) and 1.5 % of sites (10/650 unique  
267 sites). Four *de novo* mutations (2 sites) were shared between half-siblings on the maternal side,  
268 and 19 (8 sites) were shared between half-siblings on the paternal side. However, there was no  
269 significant difference between the proportion of mutations shared between pairs of individuals  
270 related on the maternal side (9 pairs, 0.70 % shared), and pairs related on their paternal side (53  
271 pairs, 0.80 % shared; Fisher's exact test  $P = 1$ ). In 6 sites, the phasing to the parent of origin  
272 confirmed that the mutation was coming from the common parent for at least one individual  
273 (Tab. 1). Moreover, the phasing was never inconsistent by attributing a shared *de novo* mutation  
274 to the other parent than the parent in common. However, 5 shared sites did appear as mosaic in  
275 the common parent, with a maximum of 5 % of the reads of the father supporting the alternative  
276 allele (4 out of 80 reads).. Nine of the *de novo* mutations (1.4 % of the total *de novo* mutations)  
277 were located in coding sequences (CDS regions), which is close to the overall proportion of  
278 coding sequences region (1.2%) in the whole macaque genome. Eight out of those eight  
279 mutations were non-synonymous.

280 **Table 1 – Six mutations shared between related individuals.**

Chrom	Position	Ref	Alt	Sibling 1	Phasing <sup>a</sup>	Sibling 2	Phasing	Sibling 3	Phasing	Sibling 4	Phasing	Common parent	Name parent
chr2	101979137	G	A	Khan	P	Delta	U					father	Smack
chr6	132663101	A	T	Amber	U	Babet	M					mother	Mayke
chr7	60635102	G	T	Sir	U	Honoria	U					father	Smack
chr7	116648579	G	A	Amber	M	Babet	U					mother	Mayke
chr9	32544257	C	T	Hoegaarde	U	Djembe	U	Babet	U	Magenta	U	father	Poseidon
chr10	65163492	G	A	Khan	P	Delta	P					father	Smack
chr15	35463257	C	T	Leffe	U	Babet	U	Magenta	U			father	Poseidon
chr17	88174686	C	A	Hoegaarde	P	Babet	P					father	Poseidon
chr19	7047030	C	T	Leffe	U	Djembe	U					father	Poseidon
chr19	15861061	C	T	Bavaria	P	Lithium	U					father	Noot

281 a: P: paternal; M: maternal; U: unphased

282

283 **Molecular dating with trio-based mutation rate**

284 Based on our inferred mutation rate and the genetic diversity of Indian rhesus macaques ( $\pi =$   
285 0.00247) estimated using whole genomic sequencing data from more than 120 unrelated wild  
286 individuals (Xue et al. 2016), we calculated the effective population size ( $N_e$ ) of rhesus  
287 macaques to be 79,874. This is similar to the  $N_e = 80,000$  estimated previously using  $\mu = 0.59 \times$   
288  $10^{-8}$  from hippocampal transcriptome and H3K4me3-marked DNA regions from 14 individuals

289 (Yuan et al. 2012), yet higher than  $N_e = 61,800$  estimated using  $\mu = 1 \times 10^{-8}$  with 120 individual  
290 full genome data (Xue et al. 2016). Assuming a generation time of 11 years and an average  
291 reproduction age of 10 years for females and 12 years for males, the yearly mutation rate of  
292 rhesus macaques was calculated based on our regression model of the number of mutations given  
293 by males and females independently, and the average callability (see equation 2 in the Methods  
294 section). As captive animals usually reproduce later than in the wild, which could impact the  
295 average mutation rate per generation, we used the regression instead of the mutation rate per  
296 generation to correct for this possible bias. The yearly mutation rate of rhesus macaques in our  
297 calculation was  $0.62 \times 10^{-9}$  per site per year, almost 1.5 times that of humans (Jónsson et al.  
298 2017).

299 Given a precise evolutionary mutation rate is essential for accurate calibration of molecular  
300 divergence events between species, we used the mutation rate we inferred for rhesus macaques to  
301 re-date the phylogeny of closely-related primate species with full genome alignment available  
302 (Moorjani et al. 2016) (Fig 4A). The molecular divergence time ( $T_D$ ) is the time since an  
303 ancestral lineage started to split into two descendant lineages, and can be inferred from the  
304 genetic divergence between the two descendant lineages and the mutation rate. The speciation  
305 time ( $T_S$ ) is a younger event that implies no more gene flow between lineages (Steiper and  
306 Young 2008). On the backward direction, the alleles of two descendant lineages are randomly  
307 sampled from their parents until going back to the most recent common ancestor (Rosenberg and  
308 Nordborg 2002). This stochastic event, known as the coalescent, depends on the population  
309 sizes, being slower in a large population (Kingman, 1982). Thus, from the divergence time, the  
310 speciation time can be inferred given the rate of coalescence (see equation 3 in the Method  
311 section). We also compared our results to those of previous dating attempts based on molecular  
312 phylogenetic trees calibrated with fossils records (Fig 4B). We found that the two methods concur  
313 for the most recent events. Specifically, we estimated that the *Macaca mulatta* and *Macaca*  
314 *fascicularis* genomes had already diverged around 3.90 million years ago (Mya) (95 % CI: 3.46  
315 – 4.46), which is slightly older than previous estimates using the molecular clock calibrated with  
316 fossils, as the molecular divergence of the two species has been estimated at 3.44 Mya with  
317 mitochondrial data (Pozzi et al. 2014) and 3.53 Mya from nuclear data (Perelman et al. 2011).

318 We estimated a speciation event between the two species 2.14 Mya after the coalescent time,  
319 also consistent with previous findings of a most common recent ancestor to the two populations  
320 of the rhesus macaque, the Chinese and the Indian population, around 1.94 Mya based on  
321 coalescent simulations (Hernandez et al. 2007). For the next node, the molecular clock seems to  
322 differ between mitochondrial and nuclear data, as the divergence time for the Papionini group  
323 into the *Papio* and *Macaca* genera has been estimated to 8.13 Mya using nuclear data (Perelman  
324 et al. 2011), and 12.17 Mya with mitochondrial data (Pozzi et al. 2014). We estimated a  
325 divergence time between these two genera of 13.17 Mya (95 % CI: 11.70 – 15.07). For earlier  
326 divergence events, our estimated divergence times are more ancient than previous reports. For  
327 instance, we estimated that the Cercopithecini and Papionini diverged 19.86 Mya (95 % CI:  
328 17.64 – 22.71), while other studies had calculated 11.55 Mya using nuclear data (Perelman et al.  
329 2011), and 14.09 Mya using mitochondrial data (Pozzi et al. 2014). Finally, the divergence  
330 between Cercopithecidae and Hominoidea has been reported between 25 and 30 Mya (Stewart  
331 and Disotell 1998; Moorjani et al. 2016), with an estimation of 31.6 Mya using the nuclear  
332 molecular clock (Perelman et al. 2011) and 32.12 Mya using the mitochondrial one (Pozzi et al.  
333 2014). Our dating of the divergence time between the Cercopithecidae and Hominoidea of 52.31  
334 Mya (95 % CI: 46.47 – 59.83) is substantially older than previous estimates. However, the  
335 estimated speciation time inferred based on the ancestral population size, suggested a speciation  
336 of the Catarrhini group into two lineages 44.50 Mya (Fig 4B).

337

## 338 **Discussion**

339

340 Despite many efforts to accurately estimate direct *de novo* mutation rates, it is still a  
341 challenging task due to the rare occurrence of *de novo* mutations, and the small sample size that  
342 is often available. Sequencing coverage is known to be a significant factor in affecting false-  
343 positive (FP), and false-negative (FN) calls when detecting *de novo* mutation (Acuna-Hidalgo  
344 et al. 2016; Tatsumoto et al. 2017). A minimal sequencing coverage at 15X was recommended  
345 for SNPs calling (Song et al. 2016). However, such coverage cannot provide sufficient power  
346 to reduce FPs because the lower depth threshold cannot preclude Mendelian violations due to

347 sequencing errors. Moreover, a larger portion of the genome would be removed in the  
348 denominator at low depth in order to reduce the FN. While most studies on direct estimation of  
349 mutation rate use 35-40X coverage (Jónsson et al. 2017; Thomas et al. 2018; Besenbacher et al.  
350 2019), their methods to reduce FP and FN differ. Some studies use the deviation from 50 % of  
351 the *de novo* mutation pass to the next generation to infer the false-positive rate (Jónsson et al.  
352 2017; Thomas et al. 2018). Others use probabilistic methods to access the callability  
353 (Besenbacher et al. 2019), or simulation of known mutation to control the pipeline quality  
354 (Pfeifer 2017). Differences in methods likely impact the calculated rate. Here, we produced  
355 sequences at 76X coverage, which allows us to apply conservative filtering processes, while  
356 still obtaining high coverage (88 %) of the autosomal genome region when inferring *de novo*  
357 mutations. To our knowledge, only one other study has used very high coverage (120X per  
358 individuals), on a single trio of chimpanzees (Tatsumoto et al. 2017). Such high coverage  
359 allowed us to achieve a false-positive rate below 10.89 % and within the regions we deemed  
360 callable, we calculated a low false-negative rate of 4.02 %.

361 Our estimated rate is higher than the  $0.58 \times 10^{-8}$  *de novo* mutations per site per generation  
362 estimated in a preprint report (Wang et al. 2020). The difference should be mainly attributed to  
363 the fact that they sequenced the offspring of younger parents (average parental age of 7.1 years  
364 for females and 7.8 years for males compared to 8.4 years for females and 12.4 years for males  
365 in this study). Using our regression from the phased mutation, we estimated a mutation rate of  
366  $0.51 \times 10^{-8}$  per site per generation, when males reproduce at 7.8 years and females reproduce at  
367 7.1 years old. Moreover, using their regression based on the age of puberty and the increase of  
368 paternal mutation per year, Wang and collaborators estimated a per generation rate of  $0.71 \times$   
369  $10^{-8}$  mutations when males reproduce at 11 years, and a yearly rate of  $0.65 \times 10^{-9}$  mutations  
370 per site per year, which is approx 5 % higher than our estimate of  $0.62 \times 10^{-9}$  (2020). This  
371 difference may be due to any combination of stochasticity, differences in *de novo* mutation rate  
372 pipelines (callability estimate, false-negative rate, and false-positive rate estimate) and different  
373 models for converting pedigree estimates to yearly rates. Our combination of high coverage  
374 data and a large number of trios allowed us to gain high confidence estimates of the germline  
375 mutation rate of rhesus macaques at around  $0.77 \times 10^{-8}$  *de novo* mutation per site per  
376 generation, ranging from  $0.49 \times 10^{-8}$  to  $1.16 \times 10^{-8}$ . This is similar to the mutation rate

377 estimated for other non-Hominidae primates;  $0.81 \times 10^{-8}$  for the owl monkey (*Aotus*  
378 *nancymaae*) (Thomas et al. 2018) and  $0.94 \times 10^{-8}$  for the African green monkey (*Chlorocebus*  
379 *sabaeus*) (Pfeifer 2017), while all Hominidae seem to have a mutation rate that is higher than  $1 \times 10^{-8}$  *de novo* mutation per site per generation (Jónsson et al. 2017; Besenbacher et al. 2019).  
380 However, if we count for the *de novo* mutation per site per year, the rate of rhesus macaque  
381 ( $0.62 \times 10^{-9}$ ) is almost 1.5-fold the human one of  $0.43 \times 10^{-9}$  mutation per sites per year  
382 (Jónsson et al. 2017).  
383 One of the main factors affecting the mutation rate within the species is the paternal age at the  
384 time of reproduction, which was attributed to the accumulation of replication-driven mutations  
385 during spermatogenesis (Drost and Lee 1995; Li et al. 1996; Crow 2000), and has been  
386 observed in many other primates (Venn et al. 2014; Jónsson et al. 2017; Marety et al. 2017;  
387 Thomas et al. 2018; Besenbacher et al. 2019). In rhesus macaques, the rate at which germline  
388 mutation increases with paternal age seems faster than in humans; we inferred 1.84 mutations  
389 more per year for the rhesus macaque father (95% CI 0.77 – 2.90 for an average callable  
390 genome of 2.35 Mb), compared to 1.51 in humans (95% CI 1.45–1.57 for an average callable  
391 genome of 2.72 Mb) (Jónsson et al. 2017). For females, there is less difference, with 0.30 more  
392 mutations per year for the mother in rhesus macaque (95% CI -0.41 – 1.02), and 0.37 more per  
393 year in human mothers (95% CI 0.32–0.43) (Jónsson et al. 2017). In rhesus macaques, males  
394 produce a larger number of sperm cells per unit of time ( $23 \times 10^6$  sperm cells per gram of testis  
395 per day (Amann et al. 1976)) than humans ( $4.4 \times 10^6$  sperm cells per gram of testis per day  
396 (Amann and Howards 1980)). This could imply a higher number of cell division per unit of  
397 time in rhesus macaques and thus more replication error during spermatogenesis. This is also  
398 consistent with the generation time effect which stipulates that an increase in generation time  
399 would decrease the number of cell division per unit of time as well as the yearly mutation rate  
400 assuming that most mutations arise from replication errors (Wu and Lit 1985; Goodman et al.  
401 1993; Ohta 1993; Li et al. 1996; Ségurel et al. 2014; Scally 2016). Indeed, humans have a  
402 generation time of 29 years, while it is 11 years for rhesus macaques. Another explanation for a  
403 higher increase of mutation rate with paternal age could be differences in the replication  
404 machinery itself. Due to higher sperm competition in rhesus macaque, the replication might be  
405 under selective pressure for fast production at the expense of replication fidelity, leading to less

407 DNA repair mechanisms. As in other primates, we found a male bias in the contribution of *de*  
408 *novo* mutations, as the paternal to maternal ratio is 4.2:1. This ratio is higher than the 2.7:1 ratio  
409 observed in mice (Lindsay et al. 2019) and slightly higher than the 4:1 ratio observed in  
410 humans (Goldmann et al. 2016; Jónsson et al. 2018; Lindsay et al. 2019). Similarly to the wild,  
411 the males of our dataset reproduced from 10 years old, which did not allow us to examine if the  
412 contribution bias was also present just after maturation. Moreover, the promiscuous behavior of  
413 rhesus macaque leads to father reproducing with younger females. Using our model to compare  
414 the contribution of each parent reproducing at the similar age, it seems that the male bias  
415 increases with the parental age, with a lower difference in contribution at the time of sexual  
416 maturation (2.3:1 for parents of 5 years old) and an increase in male to female contribution  
417 with older parents (3.6:1 for parents of 15 years old). This result differs from humans, where  
418 the male bias seems constant over time (Gao et al. 2019), but more time points in macaque  
419 would be needed to interpret the contribution over time. In rhesus macaques, the ratio of  
420 paternal to maternal contribution to the shared mutations between related individuals is 1:1,  
421 similarly to what has been shown in mice (Lindsay et al. 2019), highlighting that those  
422 mutations probably occur during primordial germ cell divisions in postzygotic stages. Our  
423 study shows many shared patterns in the *de novo* mutations among non-Hominid primates.  
424 More estimation of mammals could help understanding if these features are conserved across a  
425 broad phylogenetic scale. Moreover, further work would be needed to understand if some  
426 gamete production stages are more mutagenic in some species than others.  
427 An accurate estimation of the mutation rate is essential for the precise dating of species divergence  
428 events. We used the rhesus macaque mutation rate to estimate its divergence time with related  
429 species for which whole-genome alignments are already available and their molecular divergence  
430 times have been investigated before with other methods (Moorjani et al. 2016). The results of our  
431 direct dating method, based on molecular distances between species and *de novo* mutation rate,  
432 matched those of traditional molecular clock approaches for speciation events within 10 to 15  
433 million years. However, it often produced earlier divergence times for more ancient nodes than the  
434 molecular clock method. This incongruence might be attributed to the fossils that were used for  
435 calibration with the clock method, which has many limitations (Heads 2005; Pulquério and  
436 Nichols 2007; Steiper and Young 2008). A fossil used for calibrating a node is usually selected

437 to represent the oldest known specimen of a lineage. Still, it cannot be known if real even older  
438 specimens existed (Heads 2005). Thus, a fossil is usually assumed to be younger than the real  
439 divergence time of the species (Benton et al. 2015). Moreover, despite the error associated with  
440 the dating of a fossil itself, determining its position on a tree can be challenging and have  
441 effects on the inferred ages across the whole tree (Pulquério and Nichols 2007; Steiper and  
442 Young 2008). For instance, the Catarrhini node, marking the divergence between the  
443 Cercopithecidae and the Hominoidea, is often calibrated in primate phylogenies (Heads 2005).  
444 This node has been calibrated to approx. 25 Mya using the oldest known Cercopithecidae fossil  
445 (*Victoriapithecus*), and the oldest known Hominoidea fossil (*Proconsul*), both around 22 My  
446 old (Goodman et al. 1998). However, if the oldest Catarrhini fossil (*Aegyptopithecus*) of 33 to  
447 34 My age is used, this node could also be calibrated to 35 Mya (Stewart and Disotell 1998).  
448 Finally, instead of being an ancestral specimen of the Catarrhini, *Aegyptopithecus* has been  
449 suggested as a sister taxon to Catarrhini, which would lead to an even older calibration time for  
450 this node (Stewart and Disotell 1998).  
451 On the other hand, the direct mutation rate estimation could have produced overestimated  
452 divergence times for the Catarrhini node age compared to previous estimates (Perelman et al.  
453 2011; Pozzi et al. 2014), because the mutation rate and generation time might change cross-  
454 species and over time. It is possible that the Catarrhini ancestor would have had a faster yearly  
455 mutation rate, and/or a shorter generation time than the recent macaques. Since fossil  
456 calibration could underestimate real divergence times, molecular-based methods could  
457 overestimate it, especially by assuming a unique mutation rate to an entire clade (Steiper and  
458 Young 2008).  
459 To obtain more confidence in the estimation of divergence time, it would be necessary to have an  
460 accurate estimation of the mutation rate for various species. The estimates available today for  
461 primates vary from  $0.81 \times 10^{-8}$  per site per generation for the Owl monkey (*Aotus nancymaae*)  
462 to  $1.66 \times 10^{-8}$  per site per generation for Orangutan (*Pongo abelii*). However, the different  
463 methods and sequencing depth make it difficult to compare between species and attribute  
464 differences to biological causes or methodological ones. Therefore, more standardized methods  
465 in further studies would be needed to allow for cross-species comparison.

466

467 **Methods**

468

469 **Samples**

470 Whole blood samples (2 mL) in EDTA (Ethylenediaminetetraacetic acid) were collected from 53  
471 Indian rhesus macaques (*Macaca mulatta*) during routine health checks at the Biomedical  
472 Primate Research Centre (BPRC, Rijswijk, Netherlands). Individuals originated from two  
473 groups, with one or two reproductive males per group. After ensuring the relatedness with a test  
474 based on individual genotypes (Manichaikul et al. 2010), we ended up with 19 trios formed by  
475 33 individuals and two extended trios (for which a second generation was available). In our  
476 dataset males reproduced from 10 years old to 14.5 years old ( $\delta$  reproductive range: 4.5 years),  
477 and females from 3.5 years old to 15.7 years old ( $\varphi$  reproductive range: 12.2 years). Genomic  
478 DNA was extracted using DNeasy Blood and Tissue Kit (Qiagen, Valencia-CA, USA) following  
479 the manufacturer's instructions. BGIseq libraries were built in China National GeneBank  
480 (CNGB), Shenzhen, China. The average insert size of the samples was 230 base pairs. Whole-  
481 genome pair-ended sequencing was performed on BGISEQ500 platform, with a read length of  
482 2x100 bp. The average coverage of the raw sequences before trimming was 81X per sample (SE  
483 = 1.35). Whole-genome sequences have been deposited in NCBI (National Center for  
484 Biotechnology Information) with BioProject number PRJNA588178 and SRA submission  
485 SUB6522592.

486

487 **Reads mapping, SNPs calling, and filtering pipeline**

488 Adaptors, low-quality reads, and N-reads were removed with SOAPnuke filter (Chen et al.  
489 2017). Trimmed reads were mapped to the reference genome of rhesus macaque Mmul 8.0.1  
490 using BWA-MEM version 0.7.15 with the estimated insert size option. Only reads mapping  
491 uniquely were kept and duplicates were removed using Picard MarkDuplicates. The average  
492 coverage after mapping was 76X per individuals (SE = 1.16). Variants were called using GATK  
493 4.0.7.0 (Poplin et al. 2018); calling variants for each individual with HaplotypeCaller in BP-  
494 RESOLUTION mode; all gVCF files per sample were combined into a single one per trio using  
495 CombineGVCFs per autosomal chromosomes; finally joint genotyping was applied with

496 GenotypeGVCF. Because *de novo* mutations are rare events, variant quality score recalibration  
497 (VQSR) is not a suitable tool to filter the sites as *de novo* mutations are more likely to be filtered  
498 out as low-quality variants. Instead we used a site filtering with the following parameters: QD <  
499 2.0, FS > 20.0, MQ < 40.0, MQRankSum < - 2.0, MQRankSum > 4.0, ReadPosRankSum < -  
500 3.0, ReadPosRankSum > 3.0 and SOR > 3.0. These filters were chosen by first, running the  
501 pipeline with the site filters recommended by GATK (QD < 2.0; FS > 60.0; MQ < 40.0;  
502 MQRankSum < -12.5; ReadPosRankSum < -8.0 ; SOR > 3.0), then, doing a manual  
503 curation of the candidates *de novo* mutations on the Integrative Genome Viewer (IGV).  
504 Finally, we identified the common parameters within the apparent false-positive calls and  
505 decided to adjust the site filter to remove as many false-positives without losing much true  
506 positive calls (see the pipeline S8 Fig).

507

508 **Detection of *de novo* mutations**

509 The combination of high coverage (76X) and stringent filters reduced false-positive - calling a *de*  
510 *novo* mutation while it is not there. Thus, for each trio, we applied the following filters:

- 511 (a) Mendelian violations were selected using GATK SelectVariant and refined to only keep  
512 sites where both parents were homozygote reference (HomRef), and their offspring was  
513 heterozygote (Het).
- 514 (b) In the case of a *de novo* mutation, the number of alternative alleles seen in the offspring  
515 should account for ~ 50 % of the reads. Our allelic balance filter allowed the alternative  
516 allele to be present in 30 % to 70 % of the total number of reads (applying the same 30%  
517 cutoff as in other studies (Kong et al. 2012; Besenbacher et al. 2015; Francioli et al.  
518 2015; S9 Fig).
- 519 (c) The depth of the three individuals was filtered to be between  $0.5 \times m_{depth}$  and  $2 \times m_{depth}$ , with  
520  $m_{depth}$  being the average depth of the trio. Most of the Mendelian violations are due to  
521 sequencing errors in regions of low sequencing depth; therefore, we applied a stricter  
522 threshold on the minimum depth to avoid the peak of Mendelian violations around 20X  
523 (S10 Fig).

524  
525 (d) Finally, after analyzing each trio with different genotype quality GQ cutoff (from 10 to  
526 90), we set up a filter on the genotype quality of 60 to ensure the genotypes of the  
527 HomRef parents and the Het offspring (S11 Fig).

528 From 242,922,329 autosomal SNPs (average of 12,785,386 per trio), 2,251,363 were potential  
529 Mendelian violations found by GATK (average of 118,493 per trio), 177,227 were filtered  
530 Mendelian violations with parents HomRef and offspring Het (average of 9,328 per trio) (a),  
531 78,339 passed the allelic balance filter (average of 4,123 per trio) (b), 13,251 passed the depth  
532 filter (average of 697 per trio) (c) and 744 the genotype quality filter (average of 39 per trio)  
533 (d) (see S4 Table for details on each individual). We also remove sites where a *de novo*  
534 mutation was shared among non-related individuals (1 site shared between 4 unrelated  
535 individuals). This allowed us to detect the number of *de novo* mutations observed per trio  
536 called m. We manually checked the reads mapping quality for all *de novo* mutations sites in the  
537 Integrative Genome Viewer (IGV). And we found possible false-positive calls in 10.89 % of  
538 the sites for which the variant was absent from the offspring or also present in a parent (see S1  
539 Fig). We kept those sites for the estimation of the mutation rate, and corrected for false-positive  
540 ( $\beta = 0.1089$ ), but removed them for downstream pattern analysis. We experimentally validated  
541 the *de novo* candidates from the trio Noot (father), Platina (mother), and Lithium (offspring).  
542 Primers were designed for 39 candidates (S5 Table). PCR amplification and Sanger sequencing  
543 were conducted on each individual (protocol in Supplementary materials). On 24 sites the PCR  
544 amplification and sequencing returned high-quality results for all three individuals. A candidate  
545 was considered validated when both parents showed homozygosity for the reference allele and  
546 the offspring showed heterozygosity (S2 Fig). All sequences generated for the PCR validation  
547 have been deposited in Genbank with accession numbers MT426016 - MT426087 (S4 Table).

548 **Estimation of the mutation rate per site per generation**

549 From the number of *de novo* mutations to an estimate of the mutation rate per site per  
550 generation, it is necessary to also correct for false-negatives - not calling a true *de novo* mutation  
551 as such. To do so, we estimated two parameters: the false-negative rate and the number of

552 callable sites,  $C$ , ie. the number of sites in the genome where we would be able to call a *de*  
553 *novo* mutation if it was there. We used the BP\_RESOLUTION option in GATK to call variants  
554 for each position and thus get the exact genotype quality for each site in each individual - also  
555 sites that are not polymorphic. So unlike other studies, we do not have to rely on sequencing  
556 depth as a proxy for genotype quality at those sites. Instead, we can apply the same genotype  
557 quality threshold to the non-polymorphic sites as we do for *de novo* mutation candidate sites.  
558 This should lead to a more accurate estimate of the number of callable sites. For each trio,  $C$  is  
559 the sum of all sites where: both parents are HomRef, and the three individuals passed the depth  
560 filter (b) and the genotype quality filter (d). To correct for our last filter, the allelic balance (c),  
561 we estimated the false-negative rate  $\alpha$ , defined as the proportion of true heterozygotes sites  
562 (one parent HomRef, the other parent HomAlt and their offspring Het) outside the allelic  
563 balance threshold (S9 Fig). We also implemented in this parameter the false-negative rate of  
564 the site filters following a normal distribution (FS, MQRankSum, and ReadPosRankSum). For  
565 all trios combined, the rate of false-negatives caused by the allele balance filter and the site  
566 filters was 0.0402. To validate this false-negative rate estimation we also used a simulation  
567 method, used in other studies (Keightley et al. 2015; Pfeifer 2017). With BAMSurgeon (Ewing  
568 et al. 2015), 552 mutations were simulated across the 19 trios at random callable sites. The  
569 false-negative rate was calculated as  $1 - (\text{number of detected mutations}/\text{number of simulated}$   
570 mutations), after running the pipeline from variant calling. The mutation rate per sites per  
571 generation can then be estimated per trio with the following equation:

$$\mu = \frac{m \times (1 - \beta)}{(1 - \alpha) \times 2 \times C} \quad (1)$$

## 576 **Sex bias, ages, and relatedness**

577 *De novo* mutations were phased to their parental origin using the read-backed phasing method  
578 described in Marett et al. 2017 (script available on GitHub:  
579 <https://github.com/besenbacher/POOHA>). The method uses read-pairs that contain both a *de*  
580 *novo* mutation and another heterozygous variant, the latter of which was used to determine the

581 parental origin of the mutation if it is present in both offspring and one of the parents. The  
582 phasing allowed us to identify any parental bias in the contribution of the *de novo* mutations.  
583 Pearson's correlation test was performed between the mutation rate and ages of each parent, as  
584 well as a linear regression model for father and mother independently. A multiple linear regression  
585 model was performed to predict the mutation rate from both parental ages as predictor variables.  
586 The phased mutations were used to dissociate the effect of the parental age from one another.  
587 Because the total number of SNPs phased to the mother or the father may differ, we divided the  
588 phased *de novo* mutations found in a parent by the total SNPs phased to this parent. Only a  
589 subset of the *de novo* mutations in an offspring was phased. Thus, we applied the paternal to  
590 maternal ratio to the total number of mutations in a trio, referred to as 'upscaled' number of  
591 mutations, to predict the number of total mutations given by each parent at different ages. The  
592 two extended trios, analyzed as independent trios, also allowed us to determine if ~ 50 % of the  
593 *de novo* mutations observed in the first trio were passed on to the next generation.

594

### 595 **Characterization of *de novo* mutations**

596 From all the *de novo* mutations found, the type of mutations and their frequencies were  
597 estimated. For the mutations from a C to any base we determined if they were followed by a G to  
598 detect the CpG sites (similarly if G mutations were preceded by a C. We defined a cluster as a  
599 window of 20,000 bp to qualify how many mutations were clustered together; over all  
600 individuals, looking at related individuals, and within individuals. We simulated 663 mutations  
601 following a uniform distribution to compare with our dataset. We investigated the mutations that  
602 are shared between related individuals. Finally, we looked at the location of mutations in the  
603 coding region using the annotation of the reference genome.

604

### 605 **Molecular dating using the new mutation rate**

606 We calculated the effective population size using Watterson's estimator  $\theta = 4N_e\mu$  (Watterson  
607 1975). We estimated  $\theta$  with the nucleotide diversity  $\pi = 0.00247$  according to a recent population  
608 study (Xue et al. 2016). Thus, we calculated the effective population size as  $N_e = \frac{\pi}{4\mu}$  with  $\mu$  the  
609 mutation rate per site per generation estimated in our study. To calculate divergence time, we

610 converted the mutation rate to a yearly rate based on the regression model of the number of  
611 mutations given by each parent regarding their ages and the average callability  $C =$   
612 2,351,302,179. Given the maturation time and the high mortality due to predation, we assumed  
613 an average age of reproduction in the wild at 10 years old for females and 12 years old for males  
614 and a generation time of 11 years, also reported in another study (Xue et al. 2016). Thus, the  
615 yearly mutation rate was:

616 
$$\mu = \frac{4.6497 + 0.3042 \times \text{agematernal} + 4.8399 + 1.8364 \times \text{agepaternal} \times (1 - \beta)}{(1 - \alpha) \times 2 \times C} \quad (2)$$

617 The divergence time between species was then calculated using  $T_{divergence} = \frac{d}{2\mu}$  with  $d$  the  
618 genetic distance between species which were calculated from the whole-genome comparison  
619 (Moorjani et al. 2016) and  $\mu$  the yearly mutation rate of rhesus macaques. We also used the  
620 confidence interval at 95% of our mutation rate regression to compute the confidence interval on  
621 divergence time. Based on the coalescent theory (Kingman, 1982), the time to coalescence is  
622  $2NeG$  with  $G$  the generation time and  $Ne$  the ancestral effective population size, assumed  
623 constant over time, as shown in a previous study (Xue et al. 2016). Thus, we dated the speciation  
624 event as previously done by Besenbacher et al. 2019 with:

625 
$$T_{speciation} = T_{divergence} - 2 \times N_{e \text{ ancestor}} \times G \quad (3)$$

626

## 627 **Acknowledgments**

628 We would like to thank GenomeDK at Aarhus University for providing computational resources  
629 and supports to this study. We also thank Josefina Stiller for helpful comments on the manuscript.

630

## 631 **Data Availability Statement**

632 Whole-genome sequences have been deposited in NCBI (National Center for Biotechnology  
633 Information) with BioProject number PRJNA588178 and SRA submission SUB6522592. All  
634 sequences generated for the PCR validation have been deposited in Genbank with accession  
635 numbers MT426016 - MT426087.

636

## 637 **References**

- 638 Acuna-Hidalgo R, Bo T, Kwint MP, Van De Vorst M, Pinelli M, Veltman JA, Hoischen A, Vissers  
639 LELM, Gilissen C. 2015. Post-zygotic Point Mutations Are an Underrecognized Source of de Novo  
640 Genomic Variation. *Am. J. Hum. Genet.* 97:67–74.
- 641 Acuna-Hidalgo R, Veltman JA, Hoischen A. 2016. New insights into the generation and role of de novo  
642 mutations in health and disease. *Genome Biol.* 17.
- 643 Amann RP, Howards SS. 1980. Daily spermatozoal production and epididymal spermatozoal reserves of  
644 the human male. *J. Urol.* 124:211–215.
- 645 Amann RP, Johnson L, Thompson DL, Pickett BW. 1976. Daily Spermatozoal Production, Epididymal  
646 Spermatozoal Reserves and Transit Time of Spermatozoa Through the Epididymis of the Rhesus  
647 Monkey. *Biol. Reprod.* 15:586–592.
- 648 Awadalla P, Gauthier J, Myers RA, Casals F, Hamdan FF, Griffing AR, Côté M, Henrion E, Spiegelman  
649 D, Tarabeux J, et al. 2010. Direct measure of the de novo mutation rate in autism and schizophrenia  
650 cohorts. *Am. J. Hum. Genet.* 87:316–324.
- 651 Benton MJ, Donoghue PCJ, Asher RJ, Friedman M, Near TJ, Vinther J. 2015. Constraints on the  
652 timescale of animal evolutionary history. *Palaeontol. Electron.* 18:1–106.
- 653 Bercovitch FB, Widdig A, Trefilov A, Kessler MJ, Berard JD, Schmidtke J, Nürnberg P, Krawczak M.  
654 2003. A longitudinal study of age-specific reproductive output and body condition among male  
655 rhesus macaques, *Macaca mulatta*. *Naturwissenschaften* 90:309–312.
- 656 Besenbacher S, Hvilsom C, Marques-Bonet T, Mailund T, Schierup MH. 2019. Direct estimation of  
657 mutations in great apes reconciles phylogenetic dating. *Nat. Ecol. Evol.* [Internet] 3:286–292.  
658 Available from: <http://www.nature.com/articles/s41559-018-0778-x>
- 659 Besenbacher S, Liu S, Izarzugaza JMG, Grove J, Belling K, Bork-Jensen J, Huang S, Als TD, Li S,  
660 Yadav R, et al. 2015. Novel variation and de novo mutation rates in population-wide de novo  
661 assembled Danish trios. *Nat. Commun.* [Internet] 6:5969. Available from:  
662 <http://www.nature.com/doifinder/10.1038/ncomms6969>
- 663 Besenbacher S, Sulem P, Helgason A, Helgason H, Kristjansson H, Jonasdottir A, Jonasdottir A,  
664 Magnusson OT, Thorsteinsdottir U, Masson G, et al. 2016. Multi-nucleotide de novo Mutations in  
665 Humans. Petrov DA, editor. *PLOS Genet.* [Internet] 12:e1006315. Available from:  
666 <http://dx.plos.org/10.1371/journal.pgen.1006315>
- 667 Byskov AG. 1986. Differential of mammalian embryonic gonad. *Physiol. Rev.* 66:71–117.
- 668 Campbell CR, Tiley GP, Poelstra JW, Hunnicutt KE, Larsen PA, dos Reis M, Yoder AD. 2019. Pedigree-  
669 based measurement of the de novo mutation rate in the gray mouse lemur reveals a high mutation  
670 rate, few mutations in CpG sites, and a weak sex bias. *bioRxiv* [Internet]. Available from:  
671 <http://dx.doi.org/10.1101/724880>
- 672 Chen Y, Chen Y, Shi C, Huang Z, Zhang Y, Li S, Li Y, Ye J, Yu C, Li Z, et al. 2017. SOAPnuke: A  
673 MapReduce acceleration-supported software for integrated quality control and preprocessing of  
674 high-throughput sequencing data. *Gigascience* 7:1–6.
- 675 Crow JF. 2000. The origins, patterns and implications of human spontaneous mutation. *Nat. Rev. Genet.*

- 676 1:40–47.
- 677 Drost JB, Lee WR. 1995. Biological basis of germline mutation: Comparisons of spontaneous germline  
678 mutation rates among drosophila, mouse, and human. *Environ. Mol. Mutagen.* [Internet] 25:48–64.  
679 Available from: <http://doi.wiley.com/10.1002/em.2850250609>
- 680 Ewing AD, Houlahan KE, Hu Y, Ellrott K, Caloian C, Yamaguchi TN, Bare JC, P'ng C, Waggott D,  
681 Sabelnykova VY, Kellen MR, et al. 2015. Combining tumor genome simulation with crowdsourcing  
682 to benchmark somatic single-nucleotide-variant detection. *Nature methods.* 12(7), 623–630.
- 683 Francioli LC, Polak PP, Koren A, Menelaou A, Chun S, Renkens I. 2015. Genome-wide patterns and  
684 properties of de novo mutations in humans. *Nat. Genet.* [Internet] 47:822. Available from:  
685 <https://www.ncbi.nlm.nih.gov/pmc/articles/PMC4485564/pdf/nihms-679155.pdf>
- 686 Gao Z, Moorjani P, Sasani TA, Pedersen BS, Quinlan AR, Jorde LB, Amster G, Przeworski M. 2019.  
687 Overlooked roles of DNA damage and maternal age in generating human germline mutations. *Proc.*  
688 *Natl. Acad. Sci. U. S. A.* [Internet] 116:9491–9500. Available from:  
689 <http://www.ncbi.nlm.nih.gov/pubmed/31019089>
- 690 Gibbs RA, Rogers J, Katze MG, Bumgarner R, Weinstock GM, Mardis ER, Remington KA, Strausberg  
691 RL, Venter JC, Wilson RK, et al. 2007. Evolutionary and biomedical insights from the rhesus  
692 macaque genome. *Science (80- ).* [Internet] 316:222–234. Available from:  
693 <http://science.sciencemag.org/>
- 694 Goldmann JM, Wong WSW, Pinelli M, Farrah T, Bodian D, Stittrich AB, Glusman G, Vissers LELM,  
695 Hoischen A, Roach JC, et al. 2016. Parent-of-origin-specific signatures of de novo mutations. *Nat.*  
696 *Genet.*
- 697 Goodman M, Porter CA, Czelusniak J, Page SL, Schneider H, Shoshani J, Gunnell G, Groves CP. 1998.  
698 Toward a Phylogenetic Classification of Primates Based on DNA Evidence Complemented by  
699 Fossil Evidence. *Mol. Phylogenet. Evol.*
- 700 Goodman MF, Creighton S, Bloom LB, Petruska J, Kunkel TA. 1993. Biochemical Basis of DNA  
701 Replication Fidelity. *Crit. Rev. Biochem. Mol. Biol.* [Internet] 28:83–126. Available from:  
702 <https://www.tandfonline.com/action/journalInformation?journalCode=ibmg20>
- 703 Halldorsson B V., Palsson G, Stefansson OA, Jonsson H, Hardarson MT, Eggertsson HP, Gunnarsson B,  
704 Oddsson A, Halldorsson GH, Zink F, et al. 2019. Characterizing mutagenic effects of recombination  
705 through a sequence-level genetic map. *Science (80- ).* 363.
- 706 Heads M. 2005. Dating nodes on molecular phylogenies: A critique of molecular biogeography.  
707 *Cladistics* 21:62–78.
- 708 Hernandez RD, Hubisz MJ, Wheeler DA, Smith DG, Ferguson B, Rogers J, ... & Muzny D. 2007.  
709 Demographic histories and patterns of linkage disequilibrium in Chinese and Indian rhesus  
710 macaques. *Science, 316(5822), 240-243.*
- 711 Ho SYW, Larson G. 2006. Molecular clocks: When timesare a-changin'. *Trends Genet.* 22:79–83.
- 712 Jónsson H, Sulem P, Arnadottir GA, Pálsson G, Eggertsson HP, Kristmundsdottir S, Zink F, Kehr B,  
713 Hjorleifsson KE, Jensson BÖ, et al. 2018. Multiple transmissions of de novo mutations in families.

- 714 Nat. Genet. [Internet] 50:1674. Available from: <http://www.nature.com/articles/s41588-018-0259-9>
- 715 Jónsson H, Sulem P, Kehr B, Kristmundsdottir S, Zink F, Hjartarson E, Hardarson MT, Hjorleifsson KE,  
716 Eggertsson HP, Gudjonsson SA, et al. 2017. Parental influence on human germline de novo  
717 mutations in 1,548 trios from Iceland. Nature [Internet] 549:519–522. Available from:  
718 <http://www.nature.com/doifinder/10.1038/nature24018>
- 719 Keightley PD, Pinharanda A, Ness RW, Simpson F, Dasmahapatra KK, Mallet J, ... & Jiggins CD. 2015.  
720 Estimation of the spontaneous mutation rate in *Heliconius melpomene*. Molecular biology and  
721 evolution, 32(1), 239-243.
- 722 Kingman JFC. 1982. The coalescent. Stochastic Processes and Their Applications, 13(3), 235–248.  
723 [https://doi.org/10.1016/0304-4149\(82\)90011-4](https://doi.org/10.1016/0304-4149(82)90011-4)
- 724 Kong A, Frigge ML, Masson G, Besenbacher S, Sulem P, Magnusson G, Gudjonsson SA, Sigurdsson A,  
725 Jonasdottir A, Jonasdottir A, et al. 2012. Rate of de novo mutations and the importance of father's  
726 age to disease risk. Nature [Internet] 488:471. Available from:  
727 <https://www.nature.com/articles/nature11396.pdf>
- 728 Lapierre M, Lambert A, Achaz G. 2017. Accuracy of demographic inferences from the site frequency  
729 spectrum: The case of the yoruba population. Genetics 206:139–449.
- 730 Li WH, Ellsworth DL, Krushkal J, Chang BHJ, Hewett-Emmett D. 1996. Rates of nucleotide substitution  
731 in primates and rodents and the generation-time effect hypothesis. Mol. Phylogenet. Evol. 5:182–  
732 187.
- 733 Lindsay SJ, Rahbari R, Kaplanis J, Keane T, Hurles ME. 2019. Similarities and differences in patterns of  
734 germline mutation between mice and humans. Nat. Commun. 10:1–12.
- 735 Manichaikul A, Mychaleckyj JC, Rich SS, Daly K, Sale M, Chen WM. 2010. Robust relationship  
736 inference in genome-wide association studies. Bioinformatics 26:2867–2873.
- 737 Maretty L, Jensen JM, Petersen B, Sibbesen JA, Liu S, Villesen P, Skov L, Belling K, Theil Have C,  
738 Izarzugaza JMG, et al. 2017. Sequencing and de novo assembly of 150 genomes from Denmark as a  
739 population reference. Nature [Internet] 548:87–91. Available from:  
740 <http://www.nature.com/doifinder/10.1038/nature23264>
- 741 Moorjani P, Amorim CEG, Arndt PF, Przeworski M. 2016. Variation in the molecular clock of primates.  
742 Proc. Natl. Acad. Sci. U. S. A. [Internet] 113:10607–10612. Available from:  
743 <http://www.ncbi.nlm.nih.gov/pubmed/27601674>
- 744 Neale BM, Devlin B, Boone BE, Levy SE, Lihm J, Buxbaum JD, Wu Y, Lewis L, Han Y, Boerwinkle E,  
745 et al. 2012. Patterns and rates of exonic de novo mutations in autism spectrum disorders. Nature  
746 485:242–246.
- 747 Ohta T. 1993. An examination of the generation-time effect on molecular evolution. Proc. Natl. Acad.  
748 Sci. USA 90:10676–10680.
- 749 Oliveira S, Cooper DN, Azevedo L. 2018. De Novo Mutations in Human Inherited Disease. In: eLS. John  
750 Wiley & Sons, Ltd. p. 1–7.

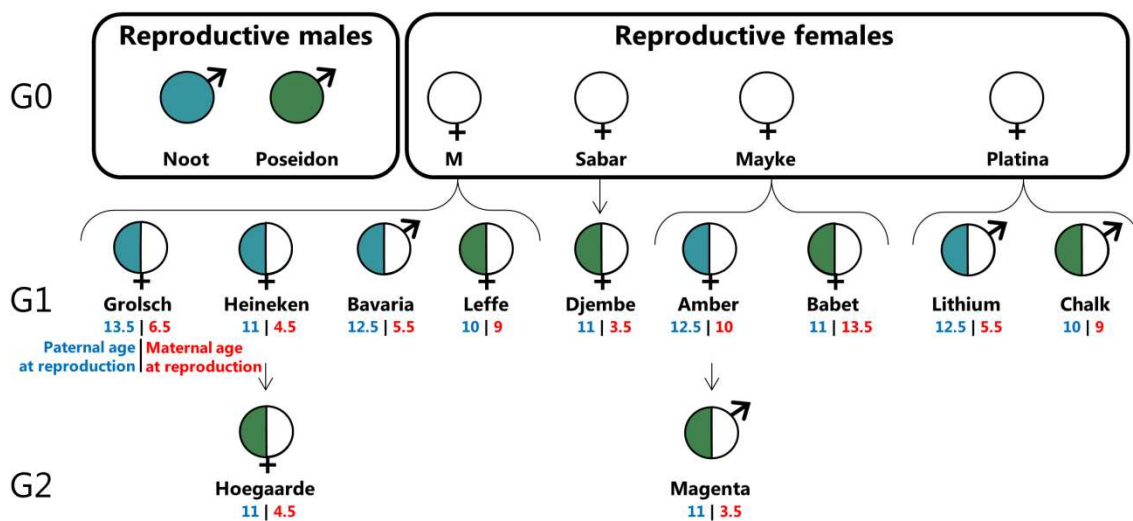
- 751 Perelman P, Johnson WE, Roos C, Seuánez HN, Horvath JE, Moreira MAM, Kessing B, Pontius J,  
752 Roelke M, Rumpf Y, et al. 2011. A Molecular Phylogeny of Living Primates. Brosius J, editor.  
753 PLoS Genet. [Internet] 7:e1001342. Available from:  
754 <https://dx.plos.org/10.1371/journal.pgen.1001342>
- 755 Pfeifer SP. 2017. Direct estimate of the spontaneous germ line mutation rate in African green monkeys.  
756 Evolution (N. Y). [Internet] 71:2858–2870. Available from:  
757 <http://doi.wiley.com/10.1111/evo.13383>
- 758 Poplin R, Ruano-Rubio V, DePristo MA, Fennell TJ, Carneiro MO, Auwera GA Van der, Kling DE,  
759 Gauthier LD, Levy-Moonshine A, Roazen D, et al. 2018. Scaling accurate genetic variant discovery  
760 to tens of thousands of samples. bioRxiv [Internet]:201178. Available from:  
761 <https://www.biorxiv.org/content/10.1101/201178v2>
- 762 Pozzi L, Hodgson JA, Burrell AS, Sterner KN, Raaum RL, Disotell TR. 2014. Primate phylogenetic  
763 relationships and divergence dates inferred from complete mitochondrial genomes. Mol.  
764 Phylogenetic Evol. 75:165–183.
- 765 Pulquero MJF, Nichols RA. 2007. Dates from the molecular clock: how wrong can we be? Trends Ecol.  
766 Evol. 22:180–184.
- 767 Rahbari R, Wuster A, Lindsay SJ, Hardwick RJ, Alexandrov LB, Turki S Al, Dominiczak A, Morris A,  
768 Porteous D, Smith B, et al. 2016. Timing, rates and spectra of human germline mutation. Nat.  
769 Genet. [Internet] 48:126–133. Available from:  
770 [http://www.nature.com/authors/editorial\\_policies/license.html#terms](http://www.nature.com/authors/editorial_policies/license.html#terms)
- 771 Rawlins RG, Kessler MJ. 1986. The Cayo Santiago Macaques: History, Behavior, and Biology. Available  
772 from:  
773 <https://books.google.fr/books?hl=en&lr=&id=3fMCzTve890C&oi=fnd&pg=PR9&dq=The+Cayo+S>  
774 antiago+macaques:+History,+behavior,+and+biology&ots=wwfUkTHWoC&sig=SUQ3CN6nFJo3h  
775 521NL6uKEzrRD4#v=onepage&q=The Cayo Santiago macaques%3A History%2C behavior%2C  
776 and biology
- 777 Roach JC, Glusman G, Smit AFA, Huff CD, Hubley R, Shannon PT, Rowen L, Pant KP, Goodman N,  
778 Bamshad M, et al. 2010. Analysis of Genetic Inheritance in a Family Quartet by Whole Genome  
779 Sequencing. Science (80-. ). [Internet] 328:636–639. Available from:  
780 <https://www.ncbi.nlm.nih.gov/pmc/articles/PMC3037280/pdf/nihms247436.pdf>
- 781 Rosenberg N. A., & Nordborg M. 2002. Genealogical trees, coalescent theory and the analysis of genetic  
782 polymorphisms. Nature Reviews Genetics, Vol. 3, pp. 380–390. <https://doi.org/10.1038/nrg795>
- 783 Scally A. 2016. Mutation rates and the evolution of germline structure. Philos. Trans. R. Soc. B Biol. Sci.  
784 [Internet] 371:20150137. Available from: <http://dx.doi.org/10.1098/rstb.2015.0137>
- 785 Schrago CG. 2014. The effective population sizes of the anthropoid ancestors of the human-chimpanzee  
786 lineage provide insights on the historical biogeography of the great apes. Mol. Biol. Evol. 31:37–47.
- 787 Ségurel L, Wyman MJ, Przeworski M. 2014. Determinants of Mutation Rate Variation in the Human  
788 Germline. Annu. Rev. Genomics Hum. Genet. [Internet] 15:47–70. Available from:  
789 <http://www.annualreviews.org/doi/10.1146/annurev-genom-031714-125740>

- 790 Song K, Li L, Zhang G. 2016. Coverage recommendation for genotyping analysis of highly heterologous  
791 species using next-generation sequencing technology. *Sci. Rep.* 6:35736.
- 792 Steiper ME, Young NM. 2008. Timing primate evolution: Lessons from the discordance between  
793 molecular and paleontological estimates. *Evol. Anthropol.* 17:179–188.
- 794 Stewart C-B, Disotell TR. 1998. Primate evolution – in and out of Africa. *Curr. Biol.* [Internet] 8:R582–  
795 R588. Available from: <https://linkinghub.elsevier.com/retrieve/pii/S0960982207003673>
- 796 Tatsumoto S, Go Y, Fukuta K, Noguchi H, Hayakawa T, Tomonaga M, Hirai H, Matsuzawa T, Agata K,  
797 Fujiyama A. 2017. Direct estimation of de novo mutation rates in a chimpanzee parent-offspring trio  
798 by ultra-deep whole genome sequencing. *Sci. Rep.* 7.
- 799 Teeling EC, Springer MS, Madsen O, Bates P, O'Brien SJ, Murphy WJ. 2005. A molecular phylogeny  
800 for bats illuminates biogeography and the fossil record. *Science* (80-. ). 307:580–584.
- 801 Thomas GWC, Wang RJ, Puri A, Rogers J, Radivojac P, Hahn MW, Thomas GWC, Wang RJ, Puri A,  
802 Harris RA, et al. 2018. Reproductive Longevity Predicts Mutation Rates in Primates. *Curr. Biol.*  
803 [Internet] 28:1–5. Available from: <https://doi.org/10.1016/j.cub.2018.08.050>
- 804 Venn O, Turner I, Mathieson I, De Groot N, Bontrop R, McVean G. 2014. Strong male bias drives  
805 germline mutation in chimpanzees. *Science* (80-. ). 344:1272–1275.
- 806 Wang H, Zhu X. 2014. De novo mutations discovered in 8 Mexican American families through whole  
807 genome sequencing. *BMC Proc.* [Internet] 8:S24. Available from:  
808 <https://www.ncbi.nlm.nih.gov/pmc/articles/PMC4143763/pdf/1753-6561-8-S1-S24.pdf>
- 809 Wang RJ, Thomas GWC, Raveendran M, Harris RA, Doddapaneni H, Muzny DM, Capitanio JP,  
810 Radivojac P, Rogers J, Hahn MW. 2020. Paternal age in rhesus macaques is positively associated  
811 with germline mutation accumulation but not with measures of offspring sociability. *Genome*  
812 *Research*, gr-255174.
- 813 Watterson GA. 1975. On the number of segregating sites in genetical models without recombination.  
814 *Theor. Popul. Biol.* 7:256–276.
- 815 Wu C-I, Lit W-H. 1985. Evolution evidence for higher rates of nucleotide substitution in rodents than in  
816 man. *Proc. Nati. Acad. Sci. USA* 82:1741–1745.
- 817 Wu FL, Strand A, Ober C, Wall JD, Moorjani P, Przeworski M. 2019. A comparison of humans and  
818 baboons suggests germline mutation rates do not track cell divisions. *bioRxiv*:844910.
- 819 Xue C, Raveendran M, Harris RA, Fawcett GL, Liu X, White S, Dahdouli M, Rio Deiros D, Below JE,  
820 Salerno W, et al. 2016. The population genomics of rhesus macaques (*Macaca mulatta*) based on  
821 whole-genome sequences. *Genome Res.* [Internet] 26:1651–1662. Available from:  
822 <http://www.ncbi.nlm.nih.gov/pubmed/27934697>
- 823 Yuan Q, Zhou Z, Lindell SG, Higley JD, Ferguson B, Thompson RC, Lopez JF, Suomi SJ, Baghal B,  
824 Baker M, et al. 2012. The rhesus macaque is three times as diverse but more closely equivalent in  
825 damaging coding variation as compared to the human. *BMC Genet.* [Internet] 13:52. Available  
826 from: <http://www.ncbi.nlm.nih.gov/pubmed/22747632>

- 827 Yuen RKC, Merico D, Cao H, Pellecchia G, Alipanahi B, Thiruvahindrapuram B, et al. 2016. Genome-  
828 wide characteristics of de novo mutations in autism. *Npj Genomic Medicine*. 1:1–10.  
829 <https://doi.org/10.1038/npjgenmed.2016.27>
- 830 Zeng K, Jackson BC, Barton HJ. 2018. Methods for estimating demography and detecting between-locus  
831 differences in the effective population size and mutation rate. *Mol. Biol. Evol.* 36:423–433.
- 832

## Figures

A



B

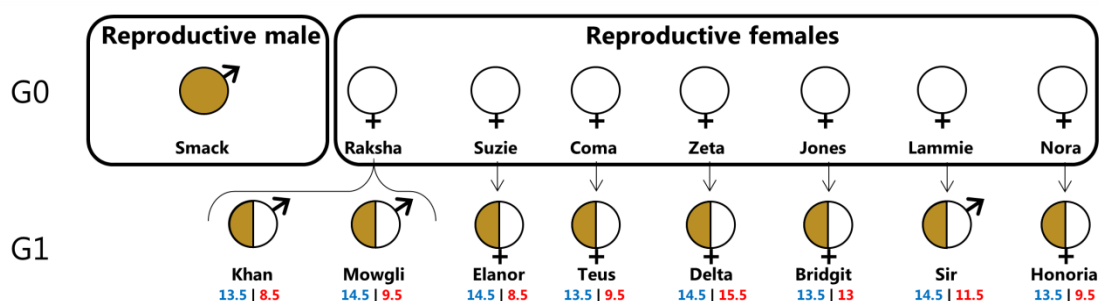


**Fig 1. Pedigree of the 19 trios used for the direct estimation of mutation rate.** A: The first group is composed of two reproductive males and four reproductive females. B: The second group contained one reproductive male and seven reproductive females. In each offspring, the color on the left corresponds to the paternal lineage and under the name are the age of the father (in blue) and mother (in red) at the time of reproduction. The reproductive ranges are 4.5 years for males and 12.2 years for females.

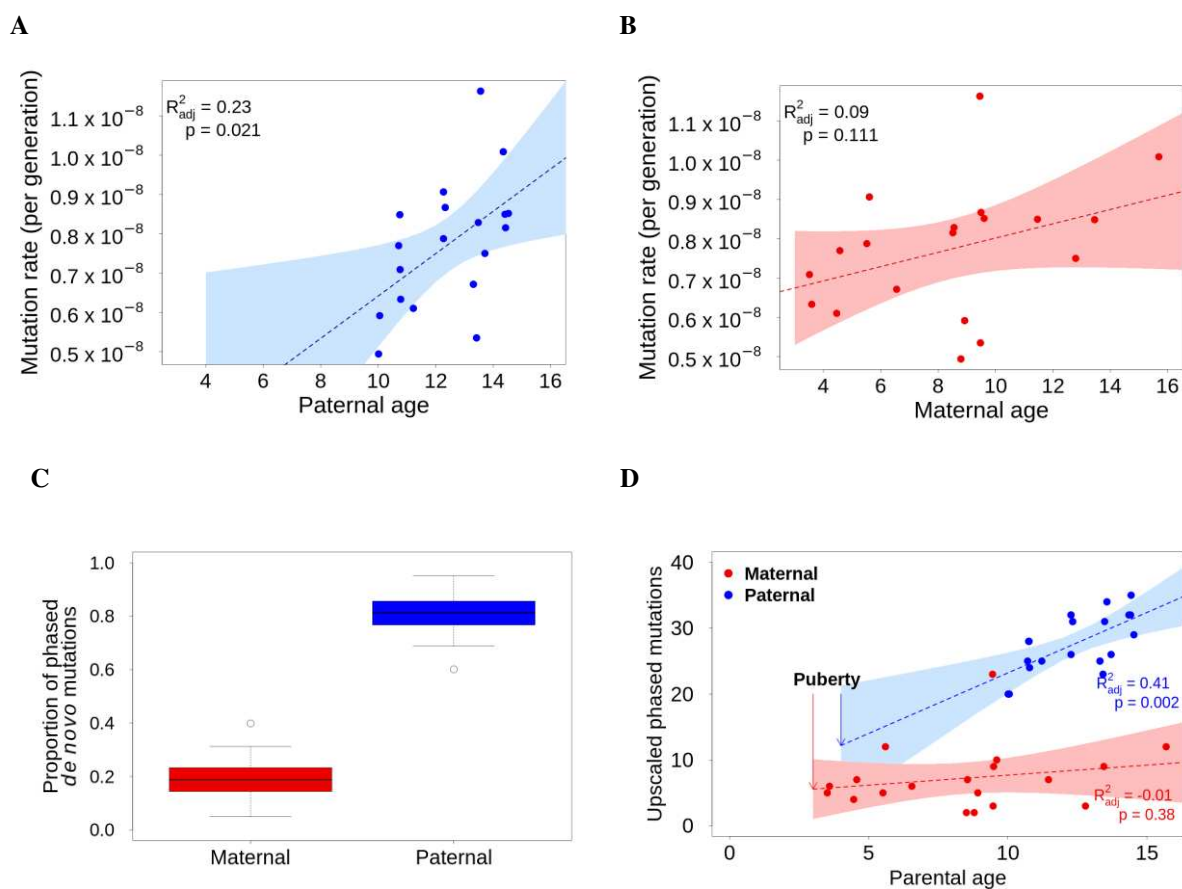


**Fig 2. Parental contribution and age effect to the *de novo* mutation rate.** A: There is a positive correlation between the mutation rate and the paternal age. B: The correlation between maternal age and mutation rate is not significant. C: Males contribute to 80.6 % of the *de novo* mutations while females contribute to 19.4 % of them. D: Upscaled number of *de novo* mutations given by each parent shows a similar contribution at the age of sexual maturation and a substantial increase with male age.

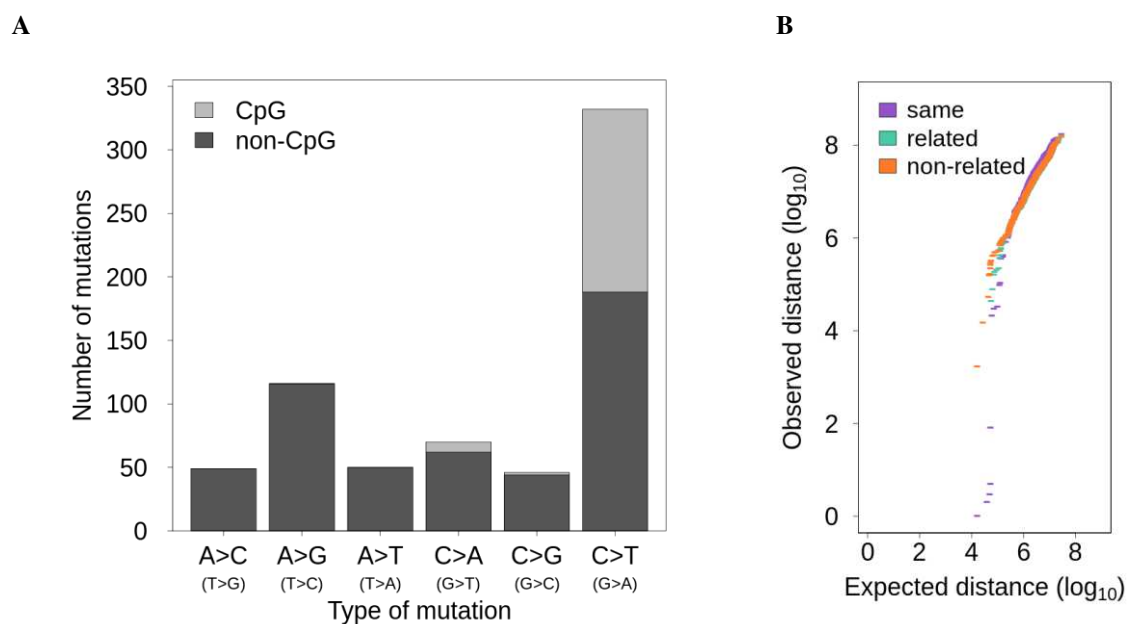


**Fig 3. Characterizations of the *de novo* mutations.** A: The type of *de novo* mutations in CpG and non-CpG sites. B: QQ-plot of the distance between *de novo* mutations compared to a uniform distribution within individuals (purple), between related individuals (green), and between non-related individuals (orange).

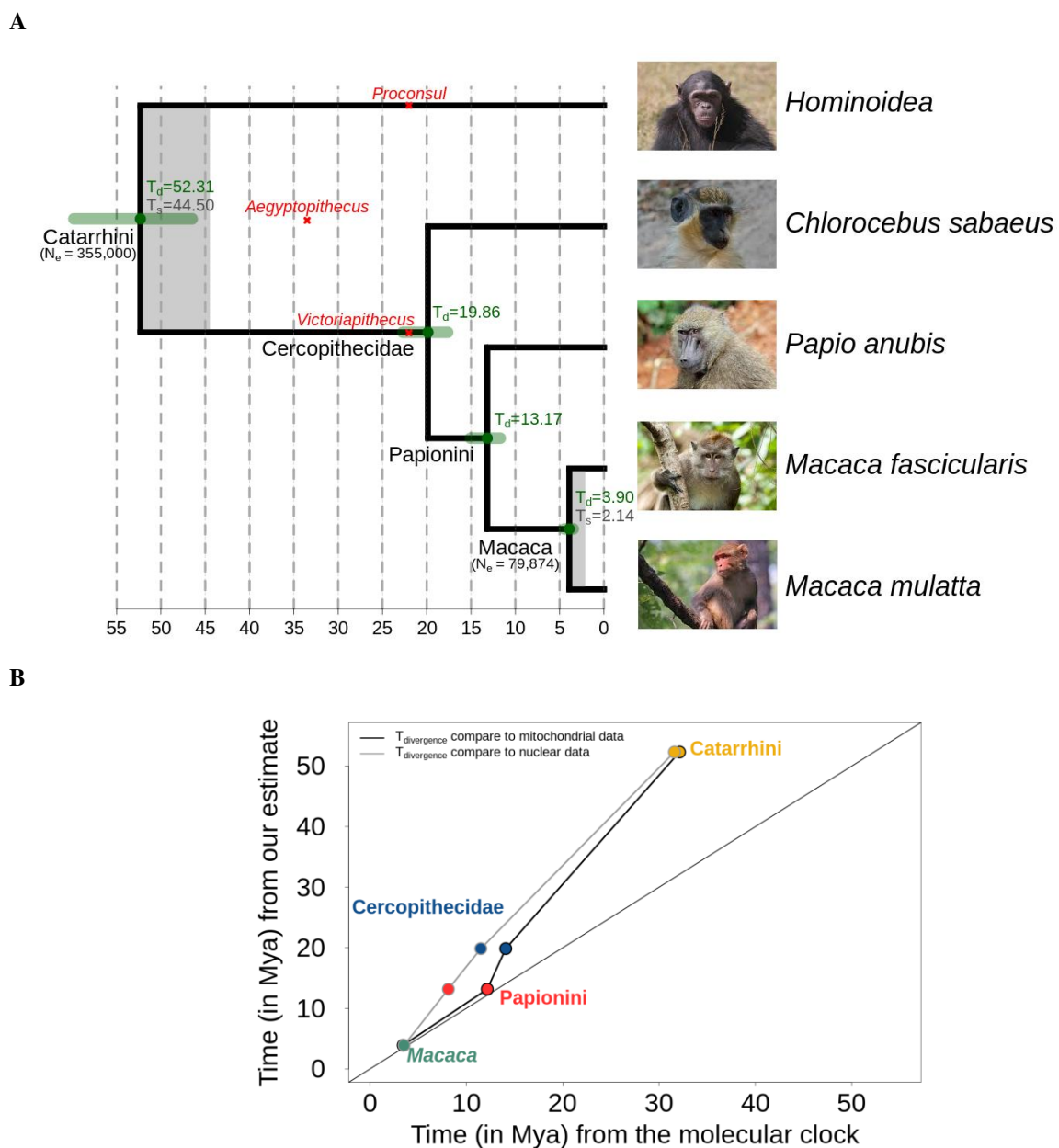


**Fig 4. Molecular dating with pedigree-based mutation rate.** A: Primates phylogeny based on the yearly mutation rate ( $0.62 \times 10^{-9}$  per site per year). In green are the confidence interval of our divergence time estimates (Td) and grey shades represent the time of speciation (Ts). The effective population sizes are indicated under the nodes (N<sub>e</sub> Macaca ancestor is our estimate of N<sub>e</sub> *Macaca mulatta* and N<sub>e</sub> Catarrhini from the literature (Schrago 2014)). B: Comparison of our divergence time and speciation time with the previous estimation using the molecular clock from mitochondrial (Pozzi et al. 2014) and nuclear data (Perelman et al. 2011) calibrated with fossils records.